© 2021. Published by The Company of Biologists Ltd | Journal of Experimental Biology (2021) 224, jeb242242. doi:10.1242/jeb.242242

RESEARCH ARTICLE

Distinct neuron phenotypes may serve object feature sensing in the electrosensory lobe of *Gymnotus omarorum*

Javier Nogueira[1,2], María E. Castelló[3], Carolina Lescano[3] and Ángel A. Caputi[1,*]

ABSTRACT

Early sensory relay circuits in the vertebrate medulla often adopt a cerebellum-like organization specialized for comparing primary afferent inputs with central expectations. These circuits usually have a dual output, carried by center ON and center OFF neurons responding in opposite ways to the same stimulus at the center of their receptive fields. Here, we show in the electrosensory lateral line lobe of Gymnotiform weakly electric fish that basilar pyramidal neurons, representing 'ON' cells, and non-basilar pyramidal neurons, representing 'OFF' cells, have different intrinsic electrophysiological properties. We used classical anatomical techniques and electrophysiological *in vitro* recordings to compare these neurons. Basilar neurons are silent at rest, have a high threshold to intracellular stimulation, delayed responses to steady-state depolarization and low pass responsiveness to membrane voltage variations. They respond to low-intensity depolarizing stimuli with large, isolated spikes. As stimulus intensity increases, the spikes are followed by a depolarizing after-potential from which phase-locked spikes often arise. Non-basilar neurons show a pacemaker-like spiking activity, smoothly modulated in frequency by slow variations of stimulus intensity. Spike-frequency adaptation provides a memory of their recent firing, facilitating non-basilar response to stimulus transients. Considering anatomical and functional dimensions, we conclude that basilar and non-basilar pyramidal neurons are clear-cut, different anatomo-functional phenotypes. We propose that, in addition to their role in contrast processing, basilar pyramidal neurons encode sustained global stimuli such as those elicited by large or distant objects while non-basilar pyramidal neurons respond to transient stimuli due to movement of objects with a textured surface.

KEY WORDS: Electric fish, ON neurons, OFF neurons, Intrinsic properties, Electric image, Early sensory processing

INTRODUCTION

Mormyriformes in Africa and Gymnotiformes in America have convergently evolved an active electric sense, which appears to be their most important sensory modality (Lissmann, 1958; Fessard, 1974; Bullock and Heiligenberg, 1986; Moller, 1995; Bullock et al., 2005). These fishes exhibit neurally commanded electrogenic organs that generate electric organ discharges (EODs). In 'pulse species' the EODs are brief and well separated by silent intervals. In 'wave species' the EOD duration is similar to its repetition interval and consequently successive EODs are fused into a continuous wave (Fessard, 1974; Bullock and Heiligenberg, 1986; Moller, 1995; Bullock et al., 2005).

The role of the EOD in this active electrosensory system is to polarize the fish's surroundings. Within the polarized field, nearby objects behave as virtual electric sources according to their intensive properties, for instance their impedance relative to the water, their extensive properties, for instance their size and shape, and their positional attributes, i.e. their location and orientation relative to the fish's coordinates (Lissmann and Machin, 1958; Heiligenberg, 1975; Rasnow, 1994; Caputi and Budelli, 2006; Nelson and MacIver, 2006; Caputi, 2017, 2020). The virtual electric field generated by a polarized object sums with the self-generated field and with the virtual fields of any other nearby objects (Migliaro et al., 2005; Pereira and Caputi, 2010).

The sempiternal repetition of the EOD produces a flow of electrosensory images on the fish's skin, which are transduced and encoded by a mosaic of cutaneous electroreceptors tuned to the time course of the self-generated, species-specific EOD (Wright, 1958; Fessard and Szabo, 1961; Bullock et al., 1961; Hopkins, 1976; Watson and Bastian, 1979; von der Emde and Bleckmann, 1994; Caputi and Aguilera, 2019). Cutaneous electroreceptors are complex organs innervated by either one (Gymnotiformes) or a few (Mormyroidea) afferent fibers that project to the electrosensory lateral line lobe (ELL), forming a kind of 'electrosensory retina' (Lissmann, 1958; Bell and Maler, 2005).

In *Gymnotus omarorum*, two types of afferent fibers give rise to two parallel electrosensory pathways, fast and slow, that project via the ELL to the mesencephalon (Réthelyi and Szabo, 1973). The fast electrosensory pathway is represented in the ELL by a single cell type, which in turn projects to a mesencephalic Jeffress-type latency comparator circuit (Castelló et al., 1998; Nogueira et al., 2006; Nogueira and Caputi, 2011, 2013, 2014; Caputi and Nogueira, 2012; Carr and Maler, 1986; Carr et al., 1986a,b; Sotelo et al., 1975). The slow electrosensory pathway forms a cerebellum-like circuit in the ELL that compares ongoing electrosensory afferences with contextual expectations, integrating sensory and motor descending inputs (Réthelyi and Szabo, 1973).

As in other early sensory relays, the ELL of all electric fish has a dual-output system (Mormyroidea: Bell and Szabo, 1986; Bell, 1986; Bell et al., 1997; Meek et al., 1999; Mohr et al., 2003; Gymnotiformes: Réthelyi and Szabo, 1973; Maler, 1979, 2009a,b; Maler et al., 1982; Shumway, 1989; Saunders and Bastian, 1984; Krahe and Maler, 2014; Clarke et al., 2015; Rodríguez-Cattáneo et al., 2020). In general, ON neurons have thick basilar dendritic trees directly stimulated by primary afferents (Meek et al., 1999; Réthelyi and Szabo, 1973; Maler, 1979). Consequently, they increase their firing probability when a local stimulus increases at the center of their receptive field (Bell et al., 1997; Saunders and Bastian, 1984; Clarke et al., 2014). Conversely, OFF neurons receive predominantly inhibitory inputs following the EOD,

[1]Departamento Neurociencias Integrativas y Computacionales, Instituto de Investigaciones Biológicas Clemente Estable, Av. Italia 3318, Montevideo, Uruguay. [2]Departamento de Histología y Embriología, Facultad de Medicina, Universidad de la República, Av. Gral Flores 2515, Montevideo, Uruguay. [3]Laboratorio Desarrollo y Evolución Neural, Instituto de Investigaciones Biológicas Clemente Estable, Av. Italia 3318, Montevideo, Uruguay.

*Author for correspondence (caputiangel@gmail.com)

J.N., 0000-0002-7818-9144; Á.A.C., 0000-0002-7238-0538

Received 15 January 2021; Accepted 1 March 2021

driven indirectly via interneurons contacted by primary afferents from the center of their receptive field (Bell et al., 1997; Saunders and Bastian, 1984; Berman and Maler, 1999).

Few articles address the functional analysis of ELL neurons in pulse Gymnotiformes, most of them dealing with their *in vivo* activity (Schlegel, 1973; Stoddard, 1997; Castelló et al., 1998; Pereira et al., 2005, 2014; Rodríguez-Cattáneo et al., 2020). Only the intrinsic properties of spherical cells in the fast electrosensory pathway have been studied *in vitro* (Nogueira et al., 2006; Nogueira and Caputi, 2011, 2013, 2014; Caputi and Nogueira, 2012; Matsushita et al., 2012).

This article reports that basilar and non-basilar pyramidal neurons not only differ in their anatomy, but also in their intrinsic electrophysiological properties and thus are clear-cut anatomo-functional neuronal phenotypes subserving the dual processing of electrosensory signals in a complementary manner. Our data also shed light on two still-unanswered crucial questions.

The first question is suggested by *in vivo* unitary recordings in the ELL of *G. omarorum* (Pereira et al., 2014; Pereira, 2016: Rodríguez-Cattáneo, 2017; Rodríguez-Cattáneo et al., 2020). In the presence of stationary metal objects, ON units increase and OFF units decrease their firing rate in the expected characteristic way (Pereira et al., 2014). However, when a moving metal object crosses through their receptive field, OFF units show paradoxical reductions in latency and increases in firing probability (Rodríguez-Cattáneo et al., 2020). We have explored how the intrinsic properties of the non-basilar neurons contribute to this paradoxical behavior.

Another important question is how the basal activity of OFF neurons is maintained in pulse Gymnotiformes. Signals transmitted by OFF neurons to higher centers are encoded in a down modulation of their repetitive basal activity, modulated by inhibitory interneurons carrying sensory afferent information. In pulse Mormyroidea, this basal activity pattern is driven by an EOD command corollary discharge (Bell et al., 1997; Mohr et al., 2003). The mechanisms in Gymnotiformes remain unknown.

We show here that non-basilar neurons show spontaneous pacemaker activity (which can be modulated both up and down) and spike-firing adaptation, enabling them to respond better to rapid sensory signal variations. In turn, basilar neurons respond better to sustained inputs as expected for classical ON output cells.

MATERIALS AND METHODS

Experiments were performed on 30 fish of the species *G. omarorum* (Richer-de-Forges et al., 2009; total fish length: 12–18 cm; unknown sex). Fish were gathered in lakes and creeks close to Montevideo (latitude 35.5 deg, longitude 55 deg) under the Authorization of the Ministry of Ganadería Agricultura y Pesca, Uruguay.

Ethics statement

Experiments were approved by the Animal Ethics Committee of the Instituto de Investigaciones Biológicas Clemente Estable (protocol number 001/03/2011). Fish care and experiments were performed under the regulations of the Comisión Honoraria de Experimentación Animal of the Universidad de la República (ordinance 4332-99) and the International Guiding Principles for Biomedical Research Involving Animals (https://olaw.nih.gov/resources/tutorial/iacuc.htm). All surgical procedures were performed under deep anesthesia. For anatomical experiments initial immersion in MS-222 (0.5 g l^{-1}; Merck, E10521-50G) was followed by perfusion of the same solution via the gills. For *in vitro* slice preparation, fish were anesthetized rapidly by immersion in a cold solution of carbogen in water (95% O_2/5% CO_2 at 5°C) (Kugino et al., 2016) before opening the skull to remove the brain.

Morphological techniques

Golgi stains and intracellular labeling with biotinylated compounds were used to characterize the morphology of basilar and non-basilar superficial pyramidal neurons.

Golgi stains

Golgi stains of the ELL were performed according to the double argentic impregnation of Ramón y Cajal and De Castro (1933). Ten fish were fixed with a dialdehyde mixture, containing glutaraldehyde 1% and paraformaldehyde 1%, in phosphate buffer (PB) (0.1 mol l^{-1}, pH 7.4). The fixative was perfused via the aorta, following saline perfusion of the vasculature. After fixation the brains were dissected out.

As mentioned before, the main axis of the ELL of pulse Gymnotiformes runs obliquely at 45 deg with respect to the brain midline. Parallel to this axis there are four somatotopic maps receiving the primary electrosensory afferent's projection. In these maps, the head is represented in the medial–rostral region and the tail is represented at the ELL pole located caudo-laterally (Castelló et al., 1998). These maps also receive descending inputs via parallel fibers running transversally. It has been reported in wave Gymnotiformes that pyramidal ELL neurons have apical dendritic trees flattened along a plane orthogonal to the parallel fibers, similar to the Purkinje neurons in the cerebellum (Saunders and Bastian, 1984). To better explore the spatial orientation of the dendritic trees of basilar and non-basilar pyramidal cells regarding these inputs, the brain was prepared so that the two ELLs were cut in orthogonal planes. A base for sectioning was cut at 45 deg (blue dotted line in Fig. 1A) with respect to the frontal plane (FP in Fig. 1A) and longitudinal axis (SP in Fig. 1A) of the brain. This procedure allowed us to cut the ELL on one side transversely (Fig. 1A, first to third light blue dotted lines) and on the other side parallel (Fig. 1A, fourth and fifth light blue dotted lines) to the ELL main axis, corresponding to the orientation of the electrosensory somatotopic multiple maps (the four pisciculi; Castelló et al., 1998; Heiligenberg and Dye, 1982).

Two brains were cut in coronal sections parallel to the frontal plane (FP in Fig. 1A). This made it possible to compare the neurons studied *in vitro* with earlier anatomical descriptions (Réthelyi and Szabo, 1973; Maler, 1979).

The prepared brainstems were then immersed in an aqueous solution of $K_2Cr_2O_7$ (5% in distilled water) for 1–2 days, followed by an aqueous solution of $AgNO_3$ (0.75%) for 1–2 days. This procedure was repeated a second time. Each whole piece was then dehydrated in increasing concentrations of ethanol, followed by acetone and embedded in Durcupan® using a series of increasing concentrations of a Durcupan® mixture diluted in acetone. After overnight in pure Durcupan® mixture (no acetone), the samples were transferred to fresh pure Durcupan® mixture and polymerized at 60°C for 2 days. The brainstems were sectioned at 100–150 µm using a sliding microtome. Preparations were observed with either a Zeiss Axioscope 50 or an Olympus IX-81 upright, bright-field microscope, and photographed at high resolution using PixeLink or Olympus microscope cameras. Selected Golgi-stained neurons were drawn by hand using a bright-field microscope equipped with a camera lucida device.

Intracellular labeling

We also explored the morphological characteristics of electrophysiologically recorded individual neurons labeled by intracellular iontophoresis of biocytin (MERK B4261-50MG). After electrophysiological recording, the slices containing labeled neurons were fixed overnight in paraformaldehyde (4% in PB), rinsed in PB and incubated in an HRP–Avidin (Vector®) conjugated

Journal of Experimental Biology (2021) 224, jeb242242. doi:10.1242/jeb.242242

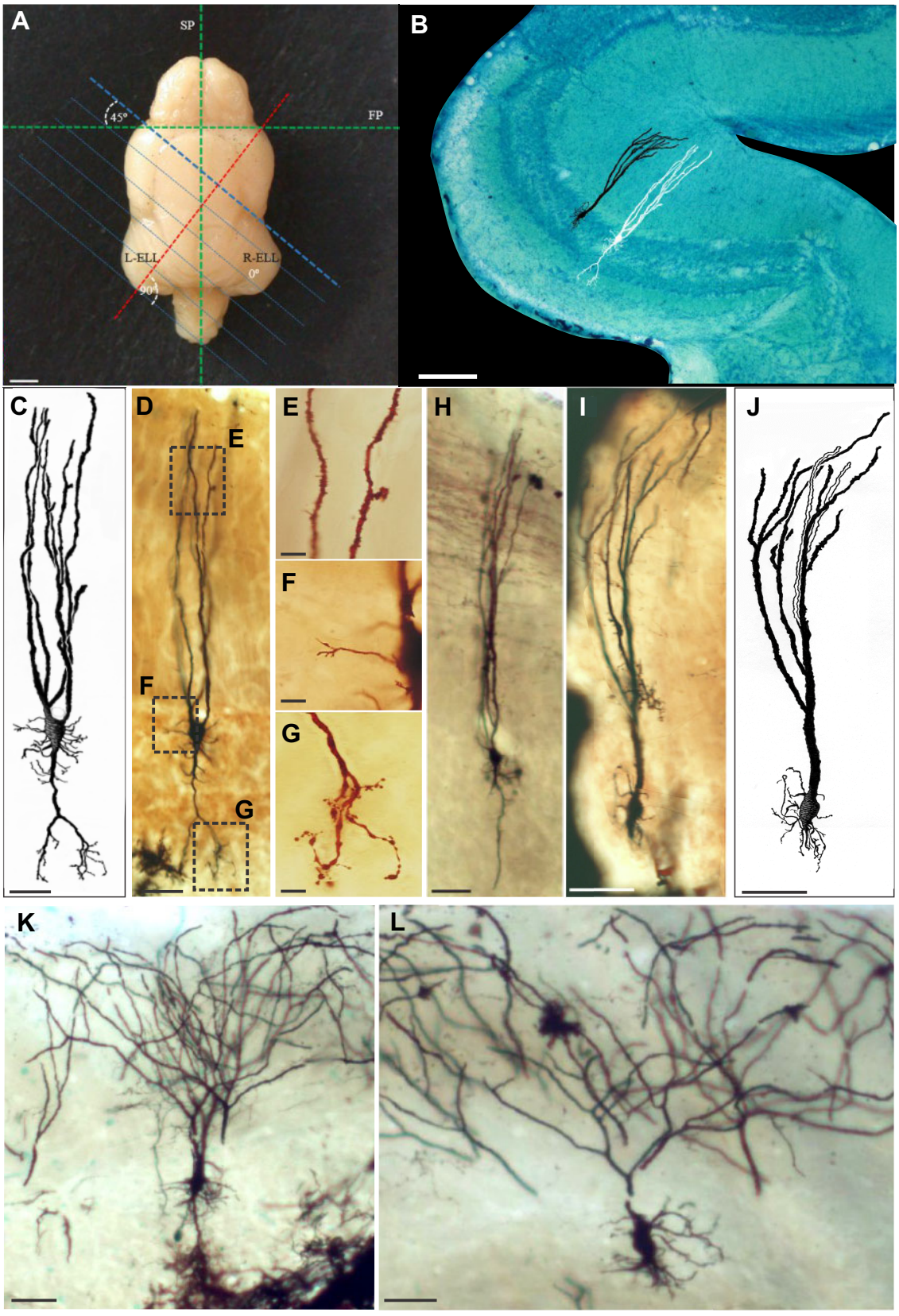

Fig. 1. See next page for legend.

Fig. 1. Morphology of basilar and non-basilar pyramidal neurons. (A) Dorsal view of brain (top: rostral) to show planes of sectioning. Green lines, transverse and longitudinal axes of the brain; red line, longitudinal axis of the left electrosensory lateral line lobe (ELL); blue line, base plane for sectioning perpendicular to the longitudinal axis of the left ELL (as shown in C–J) and parallel to the longitudinal axis of the right ELL (K,L). (B) Transverse section through left ELL. Black, non-basilar pyramidal neuron; white, basilar pyramidal neuron. (C–H,K) Golgi-stained basilar pyramidal neurons: (C) camera lucida reconstruction and (D–H,K) photomicrographs. Inset boxes in D show positions of higher magnification images in E–G. Parallel fibers in ELL dorsal molecular layer are also stained in H. (I,J) Golgi-stained non-basilar pyramidal neurons: (I) photomontage combining photomicrographs at different planes of focus and (J) camera lucida reconstruction. Scale bars (A): 1 mm; (B): 200 µm; (C,D,H–L): 25 µm; (E–G): 10 µm. FP, frontal plane; SP, longitudinal plane; L-ELL, left electrosensory lateral line lobe; R-ELL, right electrosensory lateral line lobe.

solution in the presence of 0.3% Triton X-100 for 1 h. After thorough rinsing in PB, the presence of HRP was demonstrated by the local oxidation using a Vector® SG Substrate kit (SK-4700). Slices were then counterstained with a solution of Methylene Blue (1% in distilled water), dehydrated, mounted with Canada balsam and observed as described above.

Electrophysiological techniques

Whole-cell patch recordings were performed in 200 µm thick brainstem slices cut in the coronal plane (i.e. parallel to the frontal plane marked as FP in Fig. 1A) with a Leica (1000S) vibratome. Recordings were obtained from the slices corresponding to the anterior regions of the ELL that only included the tuberous maps. After sectioning, slices were incubated for 30–60 min in a low-sodium solution containing (in mmol l^{-1}): 2 KCl, 2.6 $CaCl_2$, 1.25 $KHPO_4$, 24 $NaHCO_3$, 1.6 $MgSO_4$, 20 glucose and 201 sucrose, bubbled with carbogen (95% O_2/5% CO_2, pH 7.4). Slices were then transferred to the standard recording solution of similar composition but in which sucrose was substituted by a physiological concentration of NaCl (120 mmol l^{-1}) where they were incubated for between 2 and 6 h until they were transferred to the recording chamber placed in a fixed-stage, transmitted light microscope (Zeiss Axioskop 2 FS).

Healthy neurons were identified in the polymorphic cell layer of the ELL (Maler, 1979) using Nomarski optics under infrared illumination. Whole-cell patch recordings were obtained using 6–12 MΩ tip-polished borosilicate micropipettes filled with an intracellular solution containing (in mmol l^{-1}) 122 potassium gluconate, 2.5 $MgCl_2$, 5.6 magnesium gluconate, 0.3 $CaCl_2$, 5 Na_2ATP, 5 K-Hepes, 5 H-Hepes and 1 EGTA (pH 7.4) containing biocytin (1%) making it possible to later morphologically identify the recorded neurons.

Intracellular voltage and stimulation currents were recorded using an Axoclamp 2B amplifier (Molecular Devices, San Jose, CA, USA). After stabilizing the membrane potential, we recorded the resting activity and responses to rectangular current pulses or to extracellular electrical stimuli in the dorsal molecular layer. In 16 neurons, we explored the responses to trains of rectangular pulses lasting 500 ms, separated by 1 or 3 s, depending on the experiment. The pulse amplitude was incremented in equal magnitude steps of 30 to 80 pA, depending on the cell. In our cells, we explored the responses to hyperpolarizing and depolarizing current ramps ranging from −400 to 1000 pA s^{-1}. All experiments were performed at room temperature (19–24°C).

Electrophysiological data analysis

Systematic analysis of time course of action potentials was performed in 19 healthy recorded neurons using Octave®. We estimated the first-time derivative as the quotient of the increment of transmembrane voltage and the sampling time interval ($\Delta V/\Delta t$).

Membrane voltage and its first derivative were plotted versus time and phase portraits were constructed by plotting the derivative versus the voltage.

The following parameters were measured: (1) the presence of spontaneous pacemaker-like pre-potentials that drive regular activity at rest; (2) the maximum rising slope; (3) the peak value; (4) the maximum falling slope; (5) the interval between the peaks of the first derivative; (6) the ratio between the peaks of the first derivative; and (7) the interval between the positive peak of the action potential and the negative peak of the hyperpolarizing after-potential. We used non-parametric tests to assess whether the neuron morphological type is associated with significant differences in the median values of each of these parameters.

Neuron responsiveness to current injection in current clamp mode was assessed using 500 ms duration steps of different amplitudes in 16 neurons. During each stimulation step, two parameters were evaluated: (1) the total number of spikes over the whole duration of the stimulus; and (2) the sequence of inter-spike intervals and the spiking instantaneous frequency (IF, defined as the inverse of the inter-spike interval). Polynomial regression was employed to evaluate spike rate (number of spikes in 500 ms) as a function of current step amplitude, and IF as a function of time and current step amplitude.

Data files and Octave® codes are available from https://drive.google.com/file/d/1lRG7Ogm5mW6uqJVI9RN1SwpQmNgSO43T/view?usp=sharing

RESULTS

Morphological phenotypes

The ELL of gymnotiform weakly electric fish is a multilayered structure, in which the main output neurons subserve the fast and slow electrosensory pathway. The work presented here is focused on the two main output neuron phenotypes of the slow pathway: basilar and non-basilar pyramidal neurons. Their cell bodies are located in the polymorphic layer, and their axons project to the torus semicircularis via the lateral lemniscus (Fig. 1B; Réthelyi and Szabo, 1973; Maler, 1979, Pereira et al., 2014).

The morphology of pyramidal neuron types can be seen in Golgi-stained sections. In both neuron types, basilar (Fig. 1C–H,K) and non-basilar (Fig. 1I,J,L), somata are ovoid or pyramidal and elongated in the dorsal–ventral axis. Basilar pyramidal cells are distinguished by the presence of a single basal dendrite emerging from the ventral region of the soma and extending into the deep neuropil. In some cases, the basal dendrite has three regions: a truncated cone near the soma, often bearing short processes resembling the perisomatic dendrites; an intermediate smooth region of variable length that often bifurcates; and a terminal region with secondary and tertiary varicose dendritic branches (Fig. 1C,D,G). In other cases, the basal dendrite branches as it decreases in diameter and lacks terminal ramifications (Fig. 1H).

To evaluate perisomatic and apical dendritic fields in relation to the orientation of the pisciculi, 13 basilar neurons and six non-basilar neurons were studied in longitudinal Golgi-stained sections whereas eight of each type were studied in transverse sections with respect to the main axis of the ELL.

Perisomatic non-spiny dendrites were thin and short, and sometimes exhibited subterminal branching points (Fig. 1F). The two cell types had similar numbers of perisomatic dendrites

Journal of Experimental Biology (2021) 224, jeb242242. doi:10.1242/jeb.242242

extending further in the longitudinal than in the transverse plane (Tables S1 and S2).

Apical dendritic trees are also similar in both neuron types. The number of primary apical dendrites observed in either transverse or longitudinal planes varied from one to five in basilar neurons and from one to six in non-basilar neurons, with no significant differences between the cell types (Tables S3) Primary apical dendrites branched in the ventral molecular layer, giving rise to spiny dendrites extending up to the dorsal molecular layer. An abundance of sessile spines, in addition to pedunculated and thin spines, covering even the smallest distal branches, gave these apical dendrites a warty appearance (Fig. 1E,H–I).

The apical dendritic tree of both types of neurons fanned out rostro-caudally, parallel to the plane of the pisciculi and perpendicular to parallel fibers (Fig. 1H), appeared flattened in the transverse plane. In both basilar and non-basilar neurons, the branching angles of daughter apical dendrites were significantly larger in the longitudinal than in the transverse plane (Fig. 1C–L; Table S4). Consistently, the dendritic trees extended three times further in the longitudinal than in the transverse plane (Fig. 1C–L; Table S5).

Morphological types express distinct electrophysiological intrinsic properties

This study is based on 19 pyramidal neurons recorded with a median membrane potential of at least −55 mV. Nine of these neurons were labeled and could be anatomically identified as basilar or non-basilar pyramidal neurons, according to their similarity with Golgi stains. The action potentials were classified into two groups, taking into account the trajectory of their transmembrane voltages (Fig. 2A,B), first derivatives (Fig. 2C,D) and phase portraits (Fig. 2E,F).

Regarding the time course of the action potentials, we found that: (1) the median depolarizing overshoot in basilar neurons (+27 mV) was significantly larger than in non-basilar neurons (−0.7 mV) (Fig. 2G); (2) the median inter-peak interval of the first derivatives of the action potentials in basilar neurons (0.52 ms) was twice that observed for non-basilar neurons (0.26 ms; Fig. 2C,H); (3) the depolarizing and repolarizing slopes of the action potential were more symmetrical in non-basilar neurons (compare Fig. 2C with D, and Fig. 2I) and (4) the hyperpolarizing after-potentials were sharper in non-basilar neurons. The median interval between the peak of the spike and the hyperpolarizing after-potential in all basilar neurons (2.14 ms) was longer than that in non-basilar neurons (0.78 ms) (Fig. 2J).

Using a three-parameter criterion considering spike duration (Fig. 2H), spike symmetry (Fig. 2I) and delay of the peak of the after-hyperpolarization (Fig. 2J) together, we could infer the anatomical types of 10 other non-labeled neurons: six were classified as putative non-basilar neurons and four as putative basilar neurons.

Furthermore, in basilar neurons, the after-hyperpolarization was often followed by a depolarizing after-potential peaking about

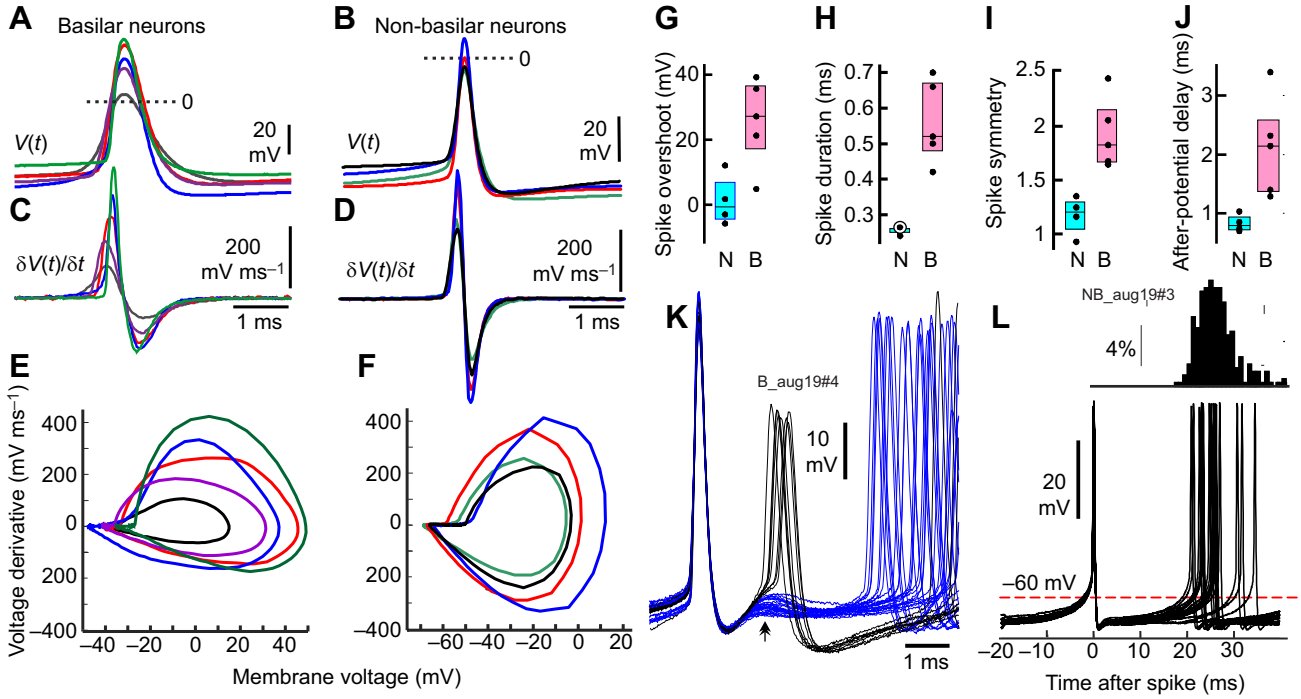

Fig. 2. The time course of the action potential distinguishes basilar from non-basilar neurons. (A,B) Superimposed action potentials of five basilar and four non-basilar neurons, respectively. Dotted line=0 mV. (C,D) First derivatives of the action potentials in A and B. (E,F) Phase portraits of the same basilar and non-basilar neurons. Individual basilar and non-basilar neurons are color coded. (G–J) Rank sum tests show that the following parameters of action potential shape are significantly larger in basilar neurons: (G) spike amplitude (P=0.037); (H) spike duration (P=0.0159); (I) spike symmetry index (P=0.0159); and (J) hyperpolarization after-potential delay (P=0.00159) [box plots show median and interquartile range: basilar (B), pink; non-basilar (N), blue]. (K) Basilar neuron action potentials show a depolarizing after-potential (black arrow, blue traces), which often gave rise to a second, smaller spike (black traces) followed by a deeper hyperpolarizing after-potential. (L) Non-basilar neuron action potentials are preceded by a pacemaker potential, which determines regular spike firing as represented in the first-order interval histogram shown above. For comparison with with other figures, labels in K and L encode the type of cell (B or NB), the recording date (e.g. aug19) and the ordinal number of the cell (#3 of #4) recording on this day. Note that these two neurons were recorded consecutively using the same bath and pipette solutions.

Journal of Experimental Biology (2021) 224, jeb242242. doi:10.1242/jeb.242242

2–4 ms after the spike peak (Fig. 2K, blue traces, arrow). In four of nine basilar neurons, this depolarizing after-potential gave rise to a smaller, phase-locked second spike also followed by an after-hyperpolarization that further hyperpolarized the membrane (Fig. 2K, black traces). Such second phase-locked spikes were not observed in non-basilar neurons (Fisher's exact test, P=0.0397).

Spontaneous activity of pyramidal neurons in brain slices

In the absence of stimulation, we observed that eight out of 10 non-basilar neurons showed a slow rising pre-potential eliciting spike firing at regular intervals. In contrast, basilar neurons were in general silent at rest although three basilar neurons were activated at irregular intervals by fluctuations of the membrane potential corresponding to synaptic activity. Thus, the presence of stereotyped pre-potentials driving repetitive firing at rest was considered a second distinctive functional feature of non-basilar neurons (Fig. 2L, Fisher's exact test on spontaneous repetitive firing versus neuron type P=0.0476).

In some non-basilar neurons (four out of 10) the basal pacemaker activity was regularly interrupted by long-lasting, quasi-stereotyped hyperpolarizing potentials (Fig. 3A). These hyperpolarizing potentials could also be recruited by extracellular stimulation, confirming their synaptic origin (Fig. 3B). Hyperpolarization of the membrane to −150 mV reduced but did not invert these long-lasting potentials. Similar quasi-periodic, long-lasting inhibitory synaptic potentials were also seen in basilar neurons (Fig. 3D).

Basilar and non-basilar neuron phenotypes show differences in excitability

Morphology and responses to an increasing series of constant current steps (500 ms duration pulses) are illustrated for typical non-basilar neurons (Fig. 4, n=10) and basilar neurons (Fig. 5, n=7). The electrophysiological profiles of the two phenotypes are compared below.

Spike rate as a function of intracellular current steps

Spike thresholds were significantly different in non-basilar and basilar neurons, illustrated by the different intersections of the abscissae in Fig. 6 (rank sum test, P=0.001). In non-basilar neurons, spike-firing rate increased monotonically with the intensity of outward current steps, increasing by one spike per second every 3–4 pA, with a mild deceleration at high stimulus intensities (Fig. 6A). Only two non-basilar neurons were not spontaneously active, and these had a very low threshold, close to zero current. In contrast, basilar neurons had a sigmoid response curve, with a higher threshold, ranging from 19 to 210 pA, and a slower increase in spike-firing rate as a function of stimulus step amplitude. When basilar neurons were stimulated at higher intensities, the spike rate became stabilized, reaching a plateau (Fig. 6B) frequency at about 140 Hz; less than half the maximal frequency observed in non-basilar neurons.

Phasic–tonic behavior of non-basilar neurons

The instantaneous frequency (IF) decreased rapidly after the start of the stimulus, approaching a steady-state value (F_0) that increased as a function of stimulus intensity (different colors in Fig. 7A) in non-basilar neurons. In Fig. 7B, the slope of the initial IF, rising as a function of stimulus intensity (red dots), is twice the slope of F_0 (black dots). To separate phasic and tonic effects we normalized IF by F_0. The curves for normalized IF as a function of time after stimulus onset, obtained with different stimulus intensities, overlapped (Fig. 7C). Moreover, the IF was well fitted by a hyperbolic function of spike timing (t) after the depolarization onset for all stimuli greater than 100 pA (Fig. 7D).

$$\mathrm{IF}(t) = F_0\left(1 + \frac{k}{t}\right), \qquad (1)$$

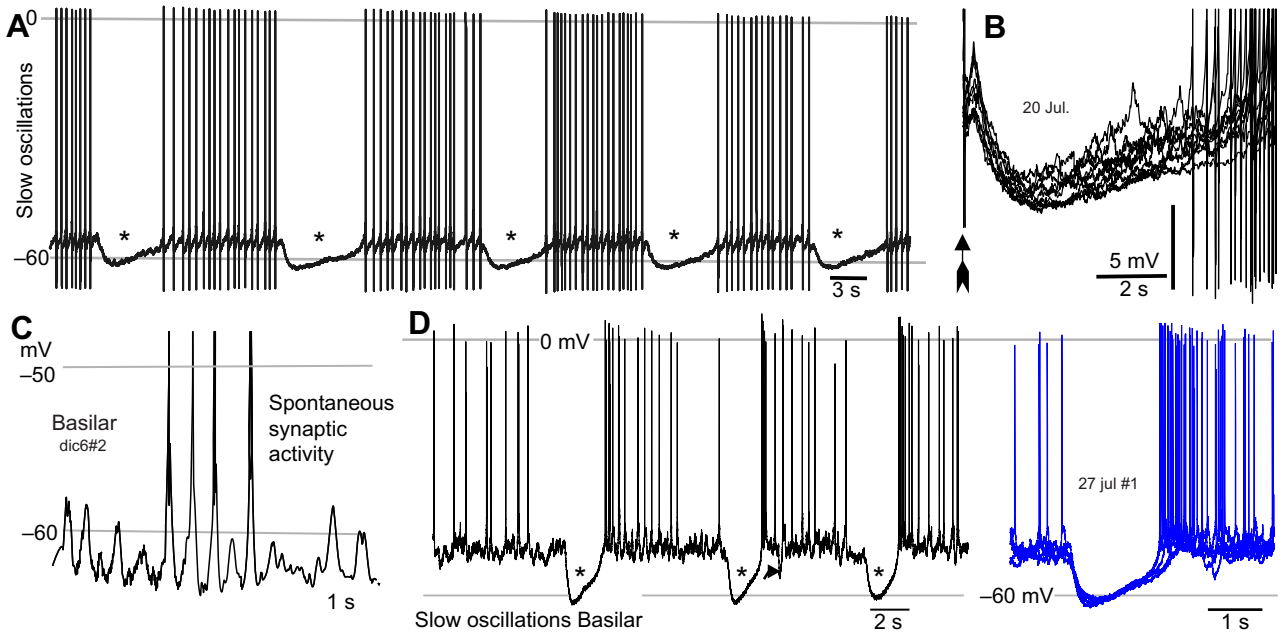

Fig. 3. Basilar and non-basilar pyramidal neurons show differences in spontaneous activity. (A) Non-basilar neurons typically fire a regular train of spikes, often interrupted by regular, slow and long-lasting inhibitory potentials (asterisks). (B) These potentials could also be recruited by extracellular stimulation. Arrow indicates the stimulus artifact. (C) Basilar neurons were either silent or showed spontaneous synaptic activity, which gave rise to isolated or paired spikes. (D) Basilar neurons also showed long-lasting inhibitory potentials (asterisks) with identical time courses (superimposed blue traces), similar to those in non-basilar neurons but with an increased probability of firing terminating the inhibition.

Journal of Experimental Biology (2021) 224, jeb242242. doi:10.1242/jeb.242242

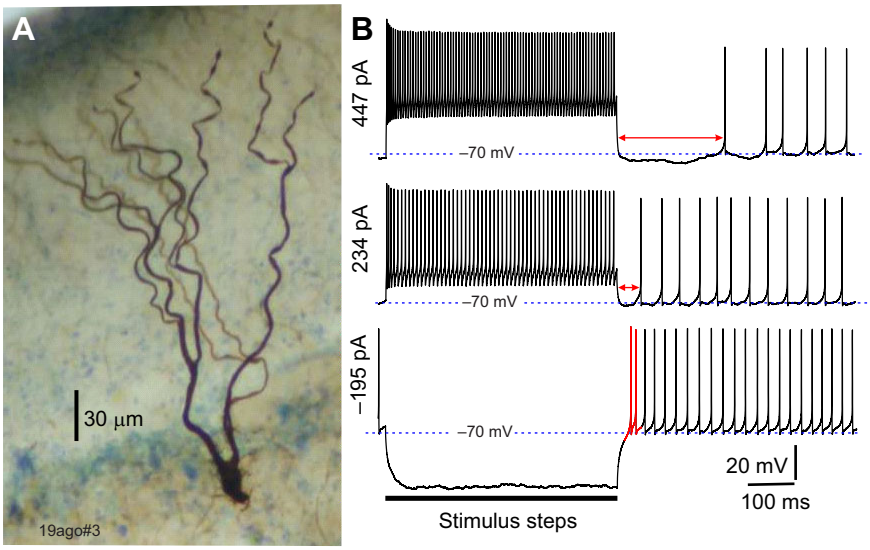

Fig. 4. Response of a typical non-basilar pyramidal neuron to a series of current steps of increasing amplitude. (A) Photomicrograph of a non-basilar neuron labeled intracellularly with biocytin. (B) Responses to hyperpolarizing and depolarizing constant current stimulus steps. Note: (1) the reduction of spike amplitude and instantaneous firing frequency several ms after depolarizing pulse onset; (2) the increase in the duration of the silent interval and the reduction in basal frequency after stimulus offset with increased current (top and middle traces: red arrows); and (3) the post-hyperpolarization rebound at the offset of the stimulus (bottom trace: red spikes). The black bar indicates the stimulus.

where k is a constant. The initial IF decayed from about twice F_0 to 1.1 times F_0 in the first 50 ms after the onset (Fig. 7D, pink area), indicating that 90% of the adaptation occurs in this period. This graph also shows that IF reached the steady state at about 200 ms (Fig. 7D, green area). Fig. 7E compares this phasic–tonic behavior in all the non-basilar neurons: the initial IF in response to 200±25 pA steps was always greater than F_0.

After the offset of a depolarizing pulse the activity of the neuron was silenced for a period that increased as a function of the spike rate at the end of the stimulus (Fig. 7F). In addition, in some non-basilar neurons the negative peak of the after-hyperpolarization was followed by a 'sag' (Fig. 7G,H, red arrow). Furthermore, in all non-basilar neurons, the offset of hyperpolarization was followed by one or two shorter inter-spike intervals (Fig. 4B, bottom row, and Fig. 7G,H, red spikes). This rebound phenomenon was absent in basilar neurons.

Adaptive tonic behavior of basilar neurons

Spike trains started with a delay following depolarizing current onset in basilar neurons, as illustrated in Fig. 8A (median latency=70 ms, n=8). Long latency activation and the differences in spiking probability during a sustained stimulus step were further explored in one neuron by applying 35 successive outward current steps of an intensity 1.5 times the threshold. Excitability increased with time during a sustained depolarization as illustrated by the superimposed responses to 10 of these stimulus steps in Fig. 8B, and the probability of spiking as a function of the latency from the step onset in Fig. 8C. At low intensities, the ratio between the mean intervals recorded during the first and last 250 ms of the stimulus step was significantly less than one, confirming that basilar neuron excitability increases as stimulus is maintained. This suggests the presence of a

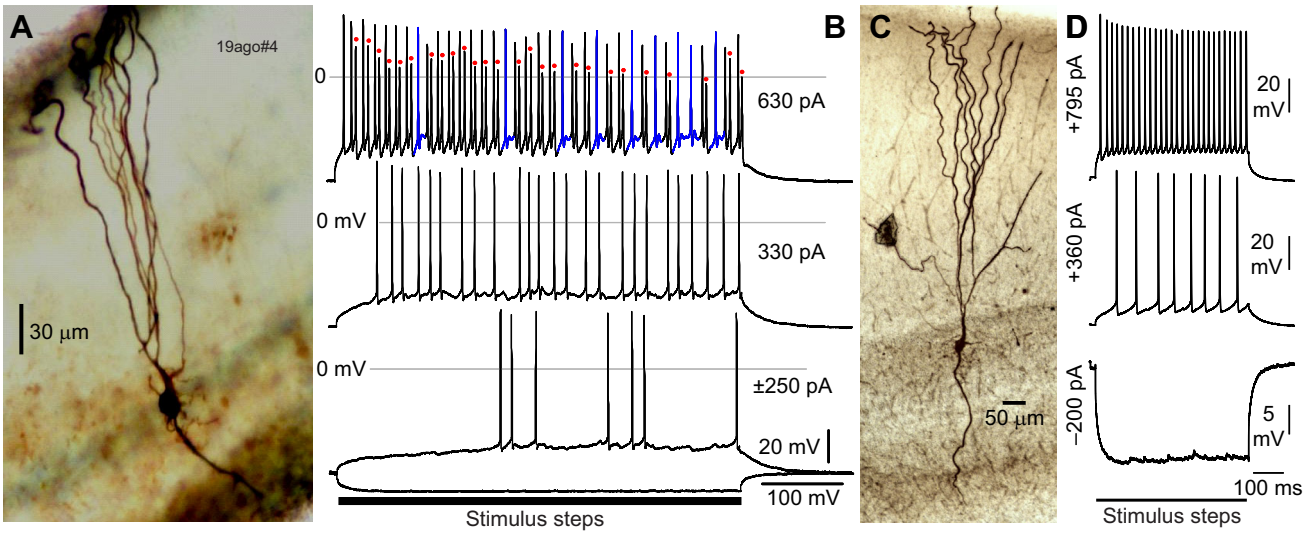

Fig. 5. Response of two typical basilar pyramidal neurons to a series of current steps of increasing amplitude. (A,C) Photomicrographs of basilar neurons intracellularly labeled with biocytin. (B) Responses of the cell in A to stimulus steps of –250 and +250 pA (bottom), +330 pA (middle) and +630 pA (top) (duration: 500 ms). Note: (1) the long delays of the first spike; (2) the irregular inter-spike intervals; and (3) two types of spikes often firing as doublets in the top trace (red dots). The isolated spikes in the top trace (blue) are similar to those observed at lower stimulus intensities but are followed by a depolarizing after-potential. (D) Responses of the cell in C to stimulus steps of –200 pA (bottom), +360 pA (middle) and +795 pA (top) (duration: 500 ms). Note the absence of doublets (upper trace) and the small synaptic activity (bottom trace). The solid black bars indicate the timing of the stimulus steps in B and D.

Journal of Experimental Biology (2021) 224, jeb242242. doi:10.1242/jeb.242242

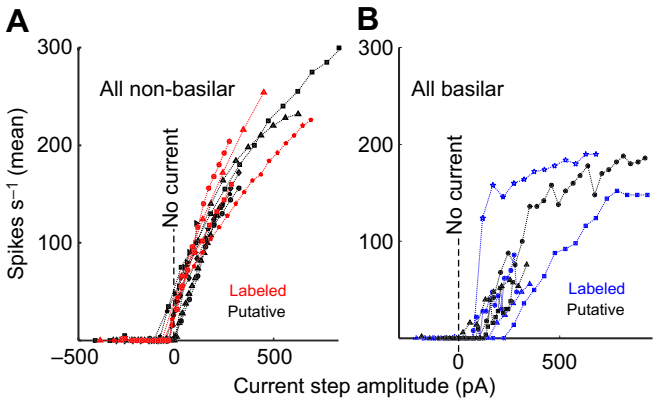

Fig. 6. Spike rate as a function of stimulus intensity in all recorded non-basilar and basilar pyramidal neurons. (A) Non-basilar neurons (red symbols, morphologically identified neurons) and (B) basilar neurons (blue symbols, morphologically identified neurons). Black symbols in both plots correspond to neurons classified according to functional criteria (see Results). Non-basilar neurons fire spontaneously and increase firing rate at about 3–4 Hz pA^{-1}. Basilar neurons start firing at relatively higher thresholds and their firing rate plateaus at about 140 Hz.

fast-activating, low-threshold conductance that shunts the membrane after the stimulus onset and inactivates with time.

The amplitude of basilar neuron action potentials decayed with the duration of the stimulus (Figs 5D and 8D). However, at high intensities the ratio between early and late spike rate converged to one, indicating that the effect of spike-firing adaptation on the firing frequency is small.

Doublet spiking is only seen in basilar neurons

Four out of nine basilar neurons discharged in doublets (Figs 2K and 5B top row) contrasting with the exclusively single spiking behavior of all non-basilar neurons. Doublet-spiking basilar neurons showed three different types of spiking patterns in response to stimuli of different current intensities. At low stimulus intensities, they fired single large spikes starting at long delays after the stimulus onset. At intermediate stimulus intensities, they fired doublets. At higher stimulus intensities, beyond a crucial point there is a transition in behavior to a constant frequency firing independent of increasing current intensity. This dynamic behavior also evolved with time during a long constant stimulus, as illustrated in Fig. 8D, where at the onset two single spikes (red) are followed by doublet firing (blue) and then, after 400 ms, by a transition to single spiking at a high constant frequency (black).

Ramp-evoked responses confirm differences in excitability between phenotypes

The responses of two non-basilar neurons and two basilar neurons to stimulation with current ramps were explored (Fig. 9). In non-basilar neurons depolarizing ramps smoothly increased the IF as a monotonic function of current intensity (blue traces in Fig. 9A,B); hyperpolarizing ramps decreased IF to zero (blue traces in Fig. 9C). The neuron of the example showed a nearly periodic activity at rest as indicated by the autocorrelation histogram (Fig. 9D). The magnitude of the change in IF was a function of stimulus intensity (Fig. 9E). As in the case of constant current stimulus, cessation of the depolarizing current caused a pause (red portion of the trace in Fig. 9A,B) while cessation of hyperpolarizing current caused spiking rebound with significantly shorter intervals separating the first two to three spikes (red spikes in Fig. 9C,F). The duration of the post-depolarization pause increased with the amplitude of the ramp and the frequency of the spiking response (Fig. 9G).

Basilar neurons showed a complex dynamic. Ramps of 100 pA s^{-1} were smoothly followed by the membrane potential up to a critical depolarization value of about 40 mV (Fig. 10A). Above this threshold, the injected current recruited a train of large, low-threshold spikes whose inter-spike intervals then increased monotonically with the instantaneous transmembrane voltage value. Towards the end of a long ramp depolarization (100 pA s^{-1}, 5 s duration), the spikes were followed by a depolarizing after-potential (DAP) of increasing amplitude but this never caused doublets. Ramps of slopes equal to or greater than 200 pA s^{-1} (Fig. 10B) showed that this depolarizing after-potential progressively increases in amplitude (Fig. 10C). The middle traces in Fig. 10C show spike numbers 1, 33, 67, 100 and 134, illustrating the increasing DAP.

There is a crucial transition point where small spikes begin to arise from the DAP producing an alternating large and small spike-firing pattern (Fig. 10B, blue spikes, magnified in 10C, right inset). As the ramp increased beyond this point the firing pattern changed again, to a nearly constant IF of about 140 Hz, which is then independent of the stimulus intensity and seems to be characteristic of this cell type (see also Fig. 6B).

The plot in Fig. 10D shows that, for 100 pA s^{-1} ramps, IF increased monotonically as a function of stimulus strength (Fig. 10D, red dots). With steeper ramp increasing at 200 mV s^{-1}, the crucial transition point and behavior shift to a maximum IF was reached at 750 pA. However, as the ramps became yet steeper, although still with the same duration, the crucial transition point (red arrows in Fig. 10D–F) came at higher current intensities, e.g. at around 800 pA for a ramp increasing at 300 mV s^{-1} and at about 950 pA for a ramp increasing at 400 mV s^{-1} (Fig. 10D–F). Thus, to reach the transition point leading to a change in firing regime required more current when the ramp depolarization was steeper.

DISCUSSION

Pyramidal neuron morphologies are similar in wave and pulse Gymnotiformes

The organization of inputs to the apical dendritic arborization, and to the perisomatic and basilar dendrites in the pulse gymnotiform *G. omarorum* is similar to that described in wave Gymnotiformes, even though the spatial orientation of the apical dendritic tree and parallel fibers appears to differ (Maler, 1979; Saunders and Bastian, 1984).

The anatomical similarity between these subtypes in wave and pulse Gymnotiformes suggests that basilar neurons are ON cells, excited by primary afferents contacting their basal dendrite (Maler, 1979, 2009a,b). Non-basilar neurons have been designated OFF cells in wave Gymnotiformes, thought to be inhibited by electrosensory input, indirectly via deep granule cells. However, Maler et al. also showed that one type of deep granule cells forms dendro-somatic and dendro-dendritic gap junctions with non-basilar pyramidal neurons thus forming a pathway potentially able to produce indirect, delayed excitation (Maler et al., 1981; Berman and Maler, 1999). This putative, indirect excitatory input, together with our physiological findings showing pacemaker activity, suggest that non-basilar neurons may be both up- and down-modulated by electrosensory input and may thus have additional functions beyond those expected for simple OFF neurons.

Spontaneous activity of basilar and non-basilar pyramidal neurons

Basilar neurons are either silent or show excitatory synaptic activity evoking isolated or paired spikes. In contrast, non-basilar neurons show a basal pacemaker membrane oscillation driving regular spiking activity. The contribution to the pacemaker activity of a hyperpolarization-activated conductance is suggested by the after-

Journal of Experimental Biology (2021) 224, jeb242242. doi:10.1242/jeb.242242

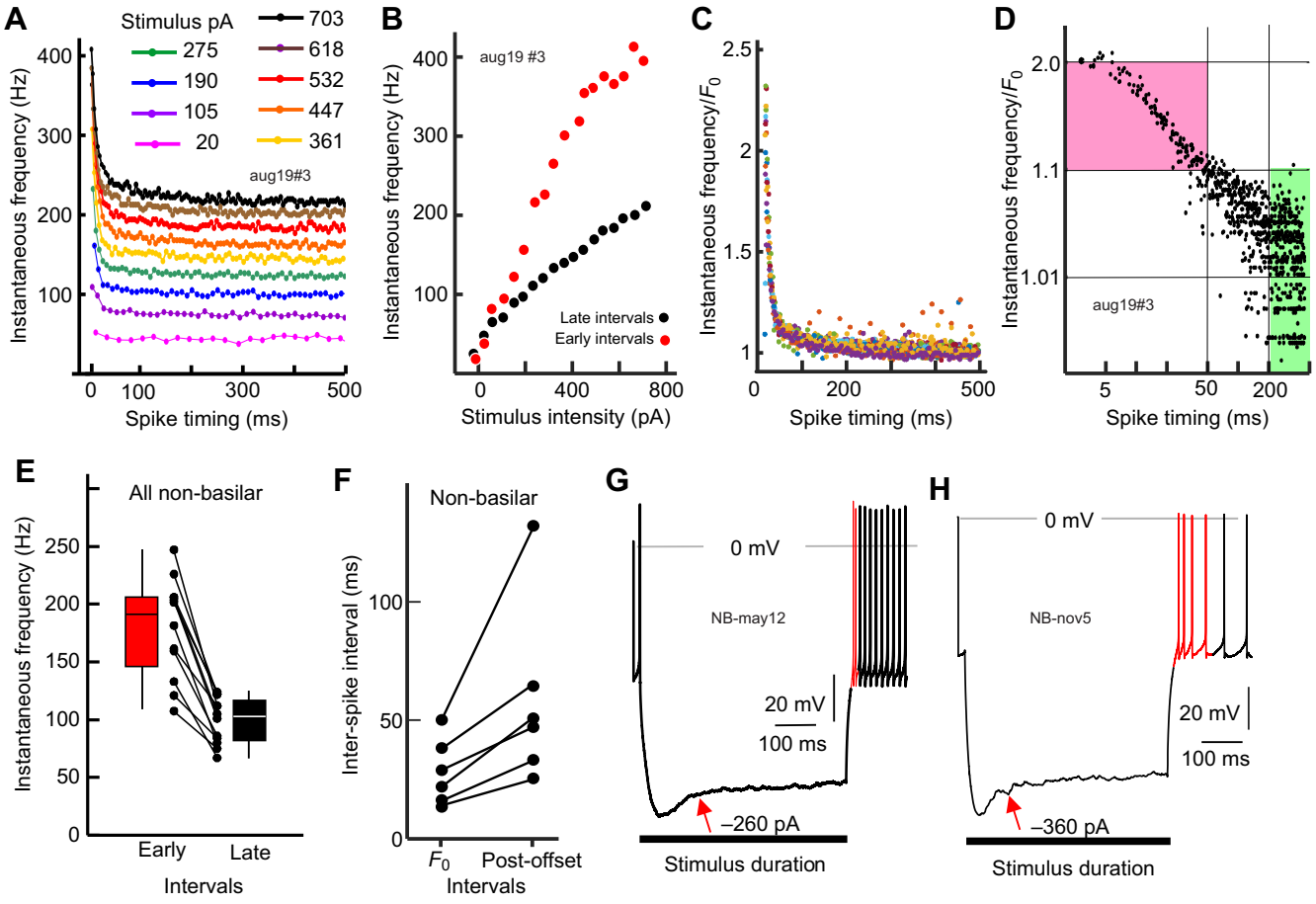

Fig. 7. Phasic–tonic responses are typical of non-basilar pyramidal neurons. (A–E) Instantaneous frequency (IF) as a function of spike timing after the stimulus onset. IF decays rapidly to a tonic-maintained frequency following a negative power law for each stimulus intensity. (A) Responses to different stimuli (color coded). (B) Mean IF measured over the first 100 ms after the onset (red) and over the last 100 ms of the 500 ms stimulus pulse as a function of stimulus intensity. (C) When normalized by the steady-state frequency (F_0), IF/F_0 curves obtained with different stimulus intensities overlap. (D) Log–log plots of (IF/F_0) −1 as a function of spike timing confirm a hyperbolic relationship (r=0.82, confidence limits 0.8–0.84, n=830 in this example, minimum r=0.59). (E) IF was significantly larger in the initial 100 ms than over the final 100 ms (constant current stimulus steps: 250–300 pA amplitude, 500 ms duration; exact probability test P=0.0019, n=10). (F) Post-offset inter-spike interval was significantly increased with respect to the steady-state frequency (F_0) (exact probability P=0.031, n=6). (G,H) Hyperpolarization sag (red arrows) and post-hyperpolarization rebound (red spikes) in two non-basilar neurons. Black bars indicate stimulus timing.

hyperpolarization ‘sag’, and by the fast spiking rebound following offset of hyperpolarizing pulses that we observed in most non-basilar neurons. Several other non-exclusive mechanisms may also subserve this type of pacemaker activity, as described, for example, in rat deep cerebellar nuclei, including recruitment of T-type calcium channels, potassium channels and a ‘tunnel effect’ of sodium channels (Dykstra et al., 2016).

A striking synaptic phenomenon observed in both phenotypes is the recurrent emergence of long-lasting hyperpolarizing potentials that periodically interrupt spontaneous firing. These potentials could also be recruited, singly, by extracellular stimulation. As it was not possible to invert these hyperpolarizing potentials, even when the membrane potential at the recording site was hyperpolarized to −150 mV, we infer that these hyperpolarizations correspond to synaptic inhibitory potentials originating electrotonically far from the current injection site. These recurrent long-lasting potentials correspond to those described previously as ‘slow oscillations’ in *in vitro* preparations in wave Gymnotiformes (Turner and Maler, 1999).

Basilar and non-basilar pyramidal neurons show differences in excitability

The differences in action potential shape, after-potentials and responsiveness between neuron types allow us to speculate on the underlying conductances shaping the intrinsic properties of each type of neuron. However, we must stress two caveats. First, different conductance combinations may support the same neuronal behavior (Ratliff et al., 2018 preprint; Alonso and Marder, 2020). Second, distinct combinations of appropriately weighted synergistic and antagonistic membrane channel features may result in the same neuronal behavior (Turrigiano et al., 1994).

K^+ conductance repertoires are distinctive features of basilar and non-basilar cells

Action potential shapes and spiking responses provide three arguments consistent with this hypothesis.

First, non-basilar neuron spikes are smaller and sharper than those in basilar neurons. This implies differences in the time constants of the action potential recovery parameters, which are most likely dominated by distinct K^+ channel repertoires characteristic for each neuron phenotype (Migliore and Shepherd, 2005). Amongst these, one must stress the potential presence of small and big calcium-activated conductances differing in their voltage dependence and time constants. As observed in other systems, small and big Ca^{2+}-activated K^+ conductances may explain the medium negative after-potential (Madison and Nicoll, 1984), and contribute to the sharp

Journal of Experimental Biology (2021) 224, jeb242242. doi:10.1242/jeb.242242

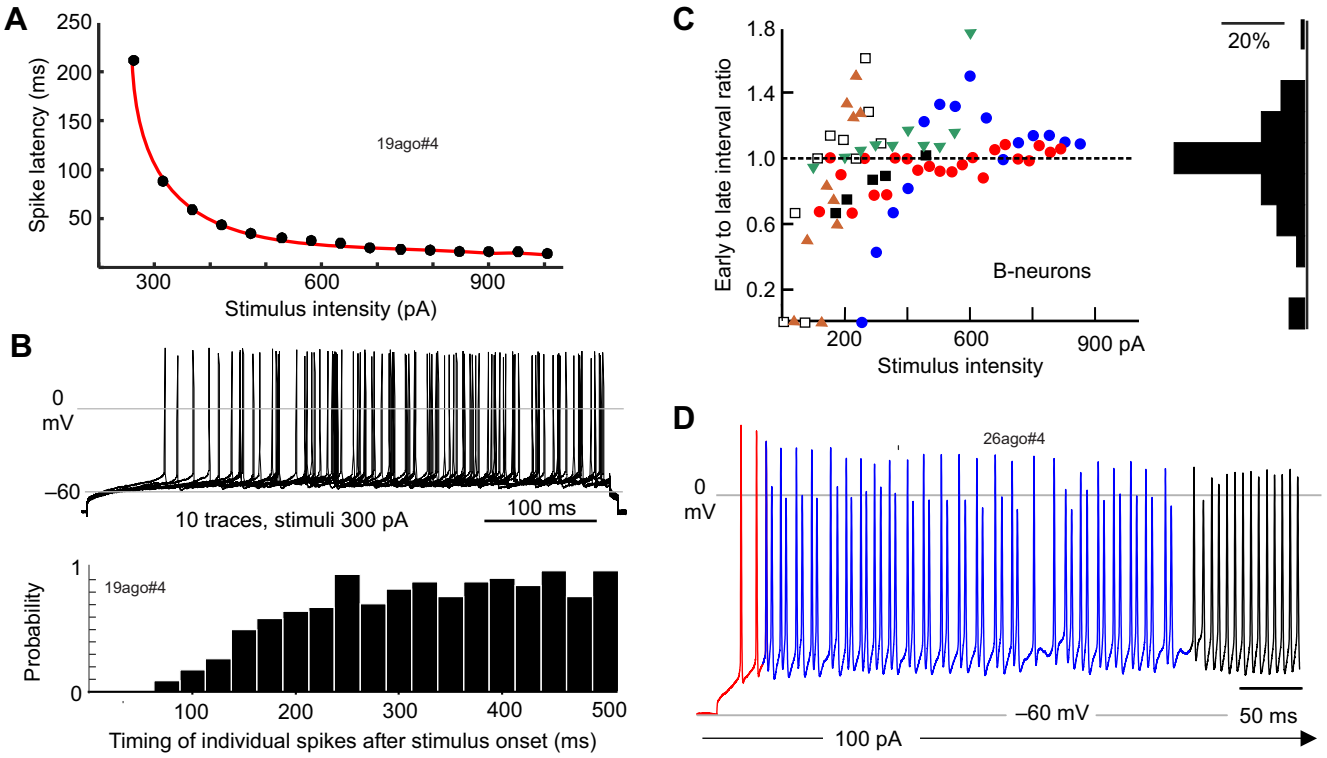

Fig. 8. Excitability of pyramidal basilar neurons. (A) The latency of the first spike is long and decays as a function of stimulus intensity. (B) The excitability is depressed transiently after the onset and recovers over time. Top: 10 traces extracted from a repetitive series of 35 steps (intensity 300 pA; duration 500 ms) separated by 1 s. Bottom: probability of spike timing after the stimulus onset (bin size 25 ms). (C) Ratio between the spike rate estimated over the first and last halves of the stimulus duration as a function of stimulus intensity. Each color corresponds to a distinct neuron. The histogram, peaking at one, shows the overall probability taking into account all neurons and stimulus intensities. (D) Response of a labeled basilar neuron to a step stimulus of 100 pA, 500 ms duration. Three firing periods may be described: isolated spikes starting firing with a long latency (red), doublets (blue), and high-frequency firing (black).

repolarization, respectively, characterizing basilar and non-basilar neurons action potential shapes (Adams et al., 1982).

Second, while the spontaneously active non-basilar neurons respond in a phasic–tonic way to depolarizing step stimuli, basilar neurons, which are silent at rest, respond with a slowly increasing firing rate. Non-basilar neurons fire regularly at rest and respond to depolarizing step onsets with an initial marked increase in IF followed by a gradual reduction, following a negative power law, to a maintained lower IF. The offset of depolarization causes a pause followed by a relaxation to the resting frequency. The non-mutually exclusive mechanisms responsible for this type of spike-frequency adaptation include (Benda and Hennig, 2008) M-type (Brown and Adams, 1980) and calcium-activated K^+ conductances (Madison and Nicoll, 1984), and slow recovery from inactivation of the fast Na^+ conductance (Fleidervish et al., 1996). Parsimony suggests that the presence of calcium-activated K^+ conductances should be explored in the search of a common factor determining adaptation in both neuron types and the accelerated repolarization and fast hyperpolarizing after-potentials of non-basilar neurons.

Third, the higher threshold of responses to depolarization and the long delays of the first evoked spikes characteristic of basilar neurons might be explained by a low-threshold-inactivating K^+ conductance (I_A) shunting membrane resistance and thus reducing excitability after the rapid change in transmembrane voltage at the beginning of a current step. This may contribute to the low-pass filtering properties of the basilar neurons.

Comparative arguments are also consistent with this hypothesis, because in wave fish, ELL output neurons exhibit a wide variety of K^+ conductances, including small calcium-activated (Ellis et al., 2008) and low threshold conductances, the expression of which is characteristic of neuron type, somatotopic map and species (Fernandez et al., 2005a,b; Mehaffey et al., 2006; Ellis et al., 2008; Mehaffey et al., 2008a).

Depolarizing after-potentials

In half of basilar neurons but in none of non-basilar neurons reported here, the after-hyperpolarization was followed by a depolarizing potential that gave rise to spike doublets. Our results in the pulse fish *G. omarorum* show that spiking discharges in doublets is a time-dependent phenomenon. Doublet spiking only occurred after rapid transitions in membrane potential, e.g. at the onset of depolarizing current steps or at transition points in fast ramps. They were not present in response to slow depolarizing ramps. This is consistent with the postulated presence of a transiently activated I_A conductance, which prevents basilar neurons from jumping immediately from silence to the high-frequency oscillatory regime observed at the end of long constant current pulses and fast stimulation ramps. A similar process was extensively studied in wave Gymnotiformes (Turner and Maler, 1999; Mehaffey et al., 2008a,b) and described as follows. A spike discharge at the somatic level back-propagates into the apical dendrite. Here, the inward current produced by the dendritic action potential acts as a current source depolarizing the soma, thus producing the depolarizing after-potential. When this current causes a sufficient depolarization, the cell fires a second spike. This activation loop shows characteristic differences among wave species (Mehaffey et al., 2008a). Although this basic loop can be the same

Journal of Experimental Biology (2021) 224, jeb242242. doi:10.1242/jeb.242242

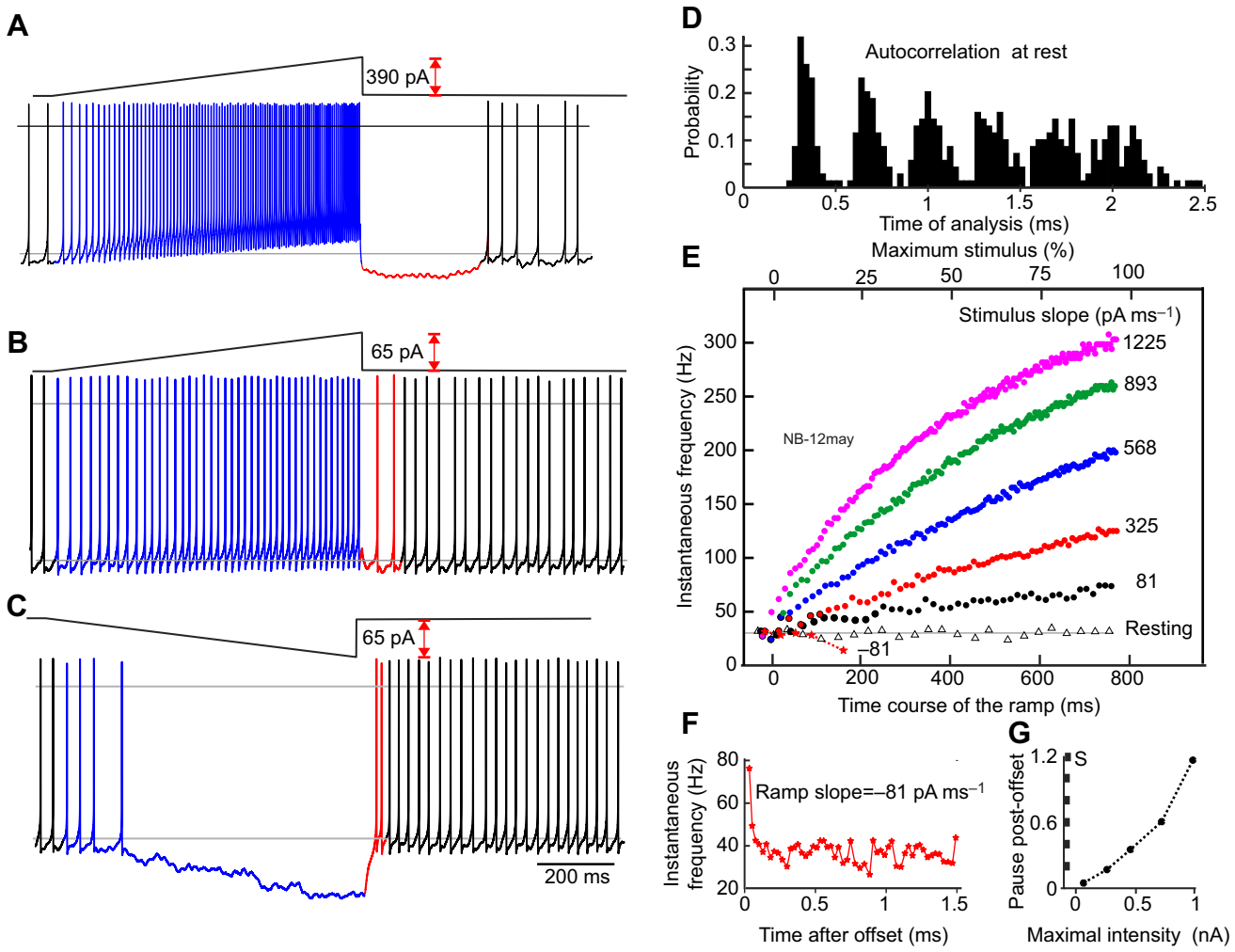

Fig. 9. Responses of non-basilar pyramidal neurons to ramps. (A–C) The periodic activity observed at rest is either (A,B) up- or (C) down-modulated by ramps of inward or outward currents, respectively. (D) Autocorrelation of the intervals at rest shows the regularity in spike firing. (E) Instantaneous frequency (IF) as a function of the time course of the ramp. Note that the intervals in the absence of stimulus (triangles) are well fitted by a horizontal line. At low inward current intensities, IF decreases to zero (red stars). At low outward current intensities (black dots), IF increases almost linearly. At higher intensities (blue, green and pink dots), the curves deviate from linear due to spike-firing adaptation. (F) The IF after the offset of a hyperpolarizing ramp decays rapidly with time. (G) The post-offset firing pause increased as a function of the maximal IF at the end of the ramp.

in all species, in pulse fish, high-intensity stimuli cause sustained firing at constant frequency instead of the burst exhausting due to dendritic Na^+ channel inactivation likely present in wave fish (Fernandez et al., 2005a,b). This may suggest species differences in the dendritic repertoire of voltage-dependent conductances.

Neuron phenotypes may serve different neurocomputational functions

In the context of the present knowledge of the circuitry and unitary data recorded in acute (Pereira et al., 2014) and freely moving fish (Rodríguez-Cattáneo et al., 2020), our present data suggest different neurocomputational roles for basilar and non-basilar neurons in the ON and OFF output channels of the ELL in pulse species. It is important to recall that field potentials and unitary recordings in the ELL of *G. omarorum* show four distinct periods of activity in the response to the EOD: an early activation (3–5 ms), followed by a brief silence (5–9 ms), then a mid-term activation (9–20 ms), and lastly a late activation (after 20 ms) (Pereira et al., 2005, 2014).

In OFF units, the post-EOD spiking histogram shows a strong depression starting 4 ms after the EOD followed by a rebounding increase in spike-firing probability in the late phase of the inter-EOD interval (Pereira et al., 2014). We suggest that this self-driven EOD-evoked downregulation in non-basilar neuron pacemaker activity is mediated by inhibitory interneurons, activated by the arrival of the sensory afferent spike train (Berman and Maler, 1998; Maler and Mugnaini, 1994). This inhibitory effect depends on the magnitude of the sensory stimulus, and is followed by an increase in spiking probability towards the end of the EOD cycle and the beginning of the next.

In addition, the observed spike-frequency adaptation and the proposed lateral excitation via gap junctions with granule cells (Maler et al., 1981; Berman and Maler, 1999) may support higher resolution in spatial and temporal contrast, and enable non-basilar neurons to encode transient components of stimuli caused by the movement of nearby textured objects surface facing the electrosensory mosaic (Caputi et al., 2011). This hypothesis is consistent with the paradoxical increase seen in the post-EOD firing rate of OFF units when a textured metal object is moved over the receptive field in a freely moving fish (Rodríguez-Cattáneo et al., 2020).

Journal of Experimental Biology (2021) 224, jeb242242. doi:10.1242/jeb.242242

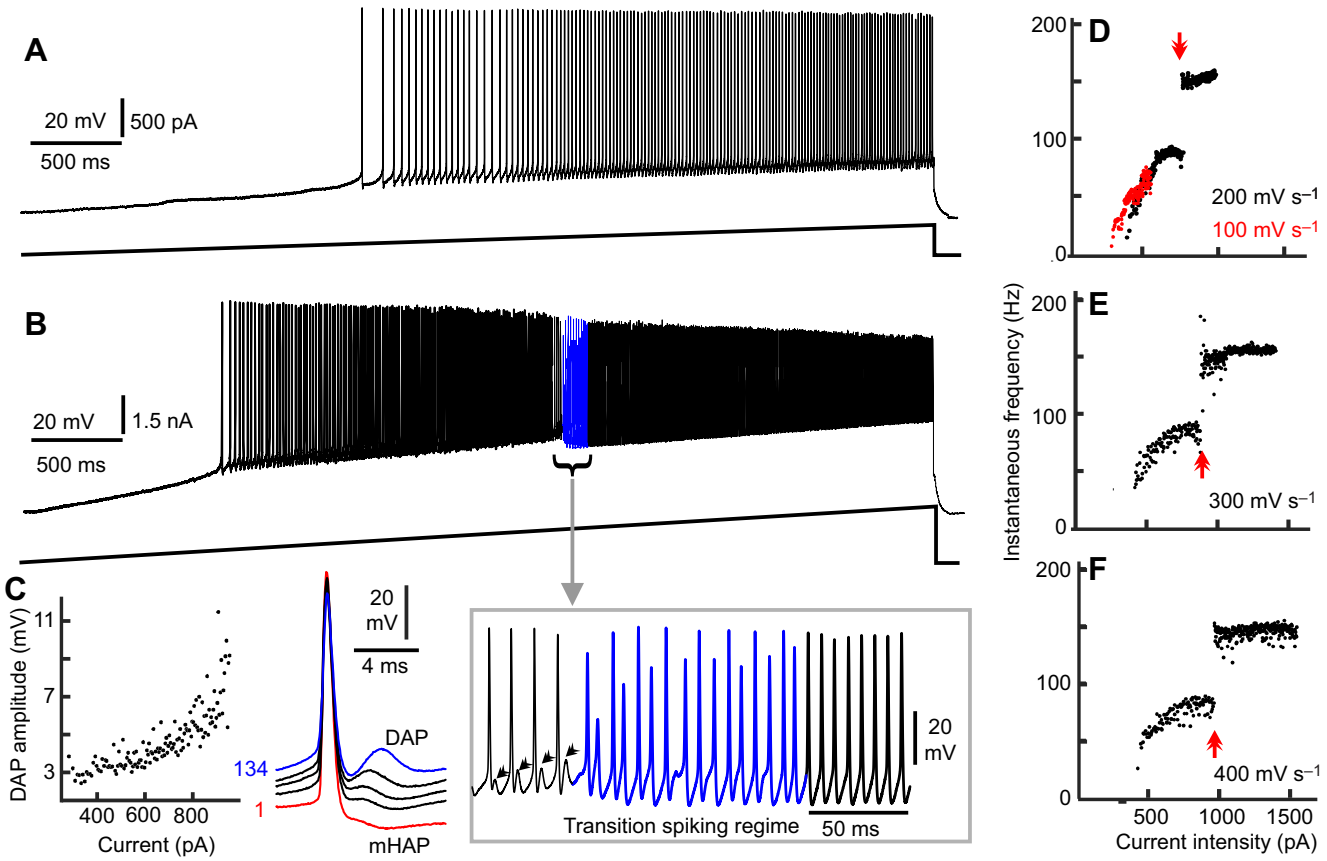

Fig. 10. Responses of basilar pyramidal neurons to ramps. (A) Response to a ramp of 100 pA s^{-1}, 5 s duration. After the spiking threshold (about 320 pA) the instantaneous frequency (IF) increased smoothly with stimulus current intensity. (B) Response of the same neuron to a ramp of 300 pA s^{-1}, 5 s duration. (C) The IF and the amplitude of the depolarizing after-potential increased as a function of current. The middle traces in C illustrating the 1st (red), 33rd, 67th, 100th (black) and 134th (blue) spikes show that the depolarizing after-potential increases progressively with ramp current. The inset in C shows detail of the transition in (B) (blue spikes) where doublet second spikes gradually increase in amplitude. (D–F) The monotonic increase of IF with instantaneous stimulus intensity corresponding to the data shown in A (red dots) contrasts with the more complex pattern observed for faster ramps (200, 300 and 400 pA s^{-1}, black dots in D–F). While red and black curves almost overlap at low-stimulation intensities, the IF jumped to a higher, constant frequency independently of the stimulus intensity above a crucial membrane potential (red arrow). DAP, depolarizing after-potential; mHAP, medium hyperpolarizing after-potential.

The electrophysiological behavior of basilar neurons can be related to that of ON units recorded *in vivo*, for which the post-EOD histogram shows an erratic early spike reflected in a small early peak at about 3–4 ms, followed by the main peak that occurs between 9 and 15 ms after the EOD (Pereira et al., 2014; Rodríguez-Cattáneo et al., 2020) and often showing doublets (fig. 5 in Pereira et al., 2014). The firing pattern may be explained by a direct synaptic depolarizing input caused by the high-frequency burst of 2–5 spikes in primary afferent fibers, arriving between 3 and 12 ms after the EOD (Rodríguez-Cattáneo et al., 2017; Caputi and Aguilera, 2019). However, the silence separating the two peaks of the histogram (4–8 ms after the EOD) is probably caused by feed-forward inhibition originating from deep oval and multipolar neurons that are also excited by primary afferent input and which project to the basilar neuron basal dendrites (Maler et al., 1981; Bastian et al., 1993; Berman and Maler, 1998, 1999). This inhibitory path is also present in *G. omarorum* (M.C. and A.A.C., unpublished data). This inhibition followed by excitation may provoke a single or a doublet of spikes depending on tonic excitation history and the contextual control made by descending electrosensory paths (Bastian, 1986; Turner and Maler, 1999; Mehaffey et al., 2008b). The low-pass responsiveness of these neurons may facilitate the evaluation of slow changes in the electric image caused by the movements of large or distant objects projecting broad images on the skin (Pereira and Caputi, 2010; Clarke et al., 2014).

Differences between ON and OFF neurons in *Gymnotus* compared with wave fish and other systems

In the visual cortex ON and OFF neurons show different receptive fields and response kinetics, suggesting a different role of ON and OFF paths in the evaluation of visual texture and movement (Jansen et al., 2019; Schiller et al., 1986). Similarly, the differences observed in the predominantly tonic and phasic–tonic responsiveness of basilar and non-basilar neurons may provide the fish with the ability of better evaluating a series of electric images corresponding to static or moving objects. This strategy at the early sensory relays is not exclusive to pulse weakly electric fish. Although different or more complex cellular mechanisms may be involved, the presence of tonic and phasic–tonic dual outputs for separately streaming the current input and its dynamic variation in early sensory relays is well known in invertebrates (Reichardt and Poggio, 1976), lower vertebrates (Lettvin et al., 1959) and more recently in the mouse retina (Kim et al., 2015).

Conclusions

Our study shows differences in the intrinsic properties of basilar and non-basilar neurons, which in the context of the known circuitry

equip them to perform movement detection in addition to their commonly accepted role in contrast evaluation. We propose that basilar and non-basilar pyramidal neurons, respectively, encode sustained global stimuli, elicited, e.g. by large or distant objects or the EODs of distant fish, and transient textural stimuli, such as those elicited by sharp edges of moving nearby objects or the complex near field of a neighboring conspecific.

Acknowledgements
The authors thank Dr Kirsty Grant for her detailed critical evaluation of the manuscript, her insightful comments and contributions on both science and language style, and the final English edition of the submitted manuscript. The authors also thank Drs Curtis Bell and Victor Han for their help with setting up the whole-cell patch recording technique, and the technical assistance of Mag. María Inés Rehermann and Sofía Ramundey during the preparation and quantification of Golgi-stained material. This work is part of the doctoral thesis studies of J.N. (Nogueira Borde, 2011).

Competing interests
The authors declare no competing or financial interests.

Author contributions
Conceptualization: A.A.C.; Methodology: J.N., A.A.C.; Software: A.A.C.; Validation: A.A.C.; Formal analysis: M.E.C., A.A.C.; Investigation: J.N., M.E.C., A.A.C.; Resources: A.A.C.; Data curation: A.A.C.; Writing - original draft: M.E.C., A.A.C.; Writing - review & editing: J.N., M.E.C., A.A.C.; Visualization: J.N., M.E.C., C.L., A.A.C.; Supervision: A.A.C.; Project administration: A.A.C.; Funding acquisition: M.E.C., A.A.C.

Funding
This work was partially supported by the following grants: Fogarty grant no. 1R03-TW05680-01 to Curtis Bell and A.A.C.; Agencia Nacional de Investigacion e Innovacion, Uruguay, grant no. FCE_1_2019_1_155541 to A.A.C. and FCE003 (no. 9036) to M.E.C.; and Programa de Desarrollo de las Ciencias Básicas (PEDECIBA) (Uruguay) PhD student allowance to J.N. Deposited in PMC for release after 12 months.

Data availability
Data files and Octave® codes are available from Google Drive: https://drive.google.com/file/d/1IRG7Ogm5mW6uqJVI9RN1SwpQmNgSO43T/view?usp=sharing

References
Adams, P. R., Brown, D. A. and Constanti, A. (1982). M–currents and other potassium currents in bullfrog sympathetic neurons. *J. Physiol.* **330**, 537-572. doi:10.1113/jphysiol.1982.sp014357

Alonso, L. M. and Marder, E. (2020). Temperature compensation in a small rhythmic circuit. *eLife* **9**, 1-24. doi:10.7554/eLife.55470

Bastian, J. (1986). Gain control in the electrosensory system mediated by descending inputs to the electrosensory lateral line lobe. *Journal of Neuroscience,* **6**, 553-562. doi:10.1523/JNEUROSCI.06-02-00553.1986

Bastian, J., Courtright, J. and Crawford, J. (1993). Commissural neurons of the electrosensory lateral line lobe of Apteronotus leptorhynchus: morphological and physiological characteristics. *J. Comp. Physiol. A* **173**, 257-274. doi:10.1007/BF00212690

Bell, C. C. (1986). Electroreception in mormyrids: central physiology. In *Electroreception* (ed. T. H. Bullock and W. Heiligenberg), pp. 375-421. New York: John Wiley and Sons.

Bell, C. C. and Maler, L. (2005). Central neuroanatomy of electrosensory systems in fish. In *Electroreception* (ed. T. H. Bullock et al.), pp. 68-111. New York, NY: Springer.

Bell, C. C. and Szabo, T. (1986). Central structures and pathways of the mormyrid electrosensory system. In *Electroreception* (ed. T. H. Bullock and W. Heiligenberg), pp. 375-421. New York: John Wiley and Sons.

Bell, C. C., Caputi, A. and Grant, K. (1997). Physiology and plasticity of morphologically identified cells in the mormyrid electrosensory lobe. *J. Neurosci.* **17**, 6409-6423. doi:10.1523/jneurosci.17-16-06409.1997

Benda, J. and Hennig, R. M. (2008). Spike-frequency adaptation generates intensity invariance in a primary auditory interneuron. *J. Comput. Neurosci.* **24**, 113-136. doi:10.1007/s10827-007-0044-8

Berman, N. J. and Maler, L. (1998). Inhibition evoked from primary afferents in the electrosensory lateral line lobe of the weakly electric fish (*Apteronotus leptorhynchus*). *J. Neurophysiol.* **80**, 3173-3196. doi:10.1152/jn.1998.80.6.3173

Berman, N. J. and Maler, L. (1999). Neural architecture of the electrosensory lateral line lobe: Adaptations for coincidence detection, a sensory searchlight and frequency-dependent adaptive filtering. *J. Exp. Biol.* **202**, 1243-1253.

Brown, D. A. and Adams, P. R. (1980). Muscarinic suppression of a novel voltage-sensitive K+ current in a vertebrate neurone. *Nature* **283**, 673-676. doi:10.1038/283673a0

Bullock, T. H. and Heiligenberg, W. (1986). *Electroreception*, pp. 722. New York, Toronto, Singapore: Wiley.

Bullock, T. H., Hagiwara, S., Kusano, K. and Negishi, K. (1961). Evidence for a category of electroreceptors in the lateral line of gymnotid fishes. *Science* **134**, 1426-1427.

Bullock, T. H., Hopkins, C. D., Popper, A. N. and Fay, R. R. (2005). *Electroreception*. New York, NY: Springer. ISBN 0-387-23192-7.

Caputi, A. A. (2017). *Active Electroreception in Weakly Electric Fish, in: Oxford Research Encyclopedia of Neuroscience*. Oxford University Press. https://oxfordre.com/neuroscience/view/10.1093/acrefore/9780190264086.001.0001/acrefore-9780190264086-e-106.

Caputi, A. A. (2020). The active electric sense of pulse gymnotiformes. In *The Senses: A Comprehensive Reference* (ed. B. Fritzsch), pp. 341-368. Elsevier.

Caputi, A. A. and Aguilera, P. A. (2019). Encoding phase spectrum for evaluating 'electric qualia. *J. Exp. Biol.* **222**, jeb191544. doi: 10.1242/jeb.191544

Caputi, A. A. and Budelli, R. (2006). Peripheral electrosensory imaging by weakly electric fish. *J. Comp. Physiol. A* **192**, 587-600. doi:10.1007/s00359-006-0100-2

Caputi, A. A. and Nogueira, J. (2012). Identifying self- and nonself-generated signals: lessons from electrosensory systems. In *Sensing in Nature. Advances in Experimental Medicine and Biology*, Vol. 739 (ed. C. López-Larrea), pp. 107-125. New York, NY: Springer.

Caputi, Á. A., Aguilera, P. A. and Pereira, A. C. (2011). Active electric imaging: body-object interplay and object's "electric texture". *PloS ONE* **6**, e22793. doi.org/10.1371/journal.pone.0022793

Carr, C. and Maler, L. (1986). Electroreception in gymnotiform fish. Central anatomy and physiology. In *Electroreception* (ed. T. H. Bullock and W. Heiligenberg), pp. 319-373. New York, NY: Wiley.

Carr, C. E., Heiligenberg, W. and Rose, G. J. (1986a). A time-comparison circuit in the electric fish midbrain. I. Behavior and physiology. *J. Neurosci.* **6**, 107-119. doi:10.1523/jneurosci.06-01-00107.1986

Carr, C. E., Maler, L. and Taylor, B. (1986b). A time-comparison circuit in the electric fish midbrain. II. Functional morphology. *J. Neurosci.* **6**, 1372-1383. doi:10.1523/jneurosci.06-05-01372.1986

Castelló, M. E., Caputi, A. and Trujillo-Cenóz, O. (1998). Structural and functional aspects of the fast electrosensory pathway in the electrosensory lateral line lobe of the pulse fish Gymnotus carapo. *J. Comp. Neurol.* **401**, 549-563.<549::AID-CNE7>3.3.CO;2-8

Clarke, S. E., Longtin, A. and Maler, L. (2014). A neural code for looming and receding motion is distributed over a population of electrosensory ON and OFF contrast cells. *J. Neurosci.* **34**, 5583-5594. doi:10.1523/JNEUROSCI.4988-13.2014

Clarke, S. E., Longtin, A. and Maler, L. (2015). Contrast coding in the electrosensory system: parallels with visual computation. *Nat. Rev. Neurosci.* **16**, 733-744. doi:10.1038/nrn4037

Dykstra, S., Engbers, J. D., Bartoletti, T. M. and Turner, R. W. (2016). Determinants of rebound burst responses in rat cerebellar nuclear neurons to physiological stimuli. *J. Physiol.* **594**, 985-1003. doi:10.1113/JP271894

Ellis, L. D., Maler, L. and Dunn, R. J. (2008). Differential distribution of SK channel subtypes in the brain of the weakly electric fish Apteronotus leptorhynchus. *J. Comp. Neurol.* **507**, 1964-1978. doi:10.1002/cne.21597

Fernandez, F. R., Mehaffey, W. H. and Turner, R. W. (2005a). Dendritic Na+ current inactivation can increase cell excitability by delaying a somatic depolarizing afterpotential. *J. Neurophysiol.* **94**, 3836-3848. doi:10.1152/jn.00653.2005

Fernandez, F. R., Mehaffey, W. H., Molineux, M. L. and Turner, R. W. (2005b). High threshold potassium channels increase gain by offsetting a frequency-dependent increase in low threshold potassium current. *J. Neurosci.* **25**, 363-371. doi:10.1523/JNEUROSCI.3950-04.2005

Fessard, A. (1974). *Electroreceptors and Other Specialized Receptors in Lower Vertebrates*. Springer-Verlag. ISBN-13: 978-3-642-65928-7.

Fessard, A. and Szabo, T. (1961). Mise en évidence d'un récepteur sensible à l'électricité dans la peau des mormyres. *Comptes Rendus Hebdomadaires des Seances de l'Academie de Sciences* **253**, 1859. doi:10.1016/j.ando.2018.06.120

Fleidervish, I. A., Friedman, A. and Gutnick, M. J. (1996). Slow inactivation of Na+ current and slow cumulative spike adaptation in mouse and guinea-pig neocortical neurones in slices. *J. Physiol.* **493**, 83-97. doi:10.1113/jphysiol.1996.sp021366

Heiligenberg, W. (1975). Theoretical and experimental approaches to spatial aspects of electrolocation. *J. Comp. Physiol.* **103**, 247-272. doi:10.1007/BF00612021

Heiligenberg, W. and Dye, J. (1982). Labelling of electroreceptive afferents in a gymnotoid fish by intracellular injection of HRP: The mystery of multiple maps. *J. Comp. Physiol.* **148**, 287-296. doi:10.1007/BF00679013

Hopkins, C. D. (1976). Stimulus filtering and electroreception: Tuberous electroreceptors in three species of Gymnotoid fish. *J. Comp. Physiol.* **111**, 171-207. doi:10.1007/BF00605531
Jansen, M., Jin, J., Li, X., Lashgari, R., Kremkow, J., Bereshpolova, Y., Swadlow, H. A., Zaidi, Q. and Alonso, J. M. (2019). Cortical balance between on and off visual responses is modulated by the spatial properties of the visual stimulus. *Cereb. Cortex* **29**, 336-355. doi:10.1093/cercor/bhy221
Kim, T., Soto, F. and Kerschensteiner, D. (2015). An excitatory amacrine cell detects object motion and provides feature-selective input to ganglion cells in the mouse retina. *ELife* **4**, e08025. doi.org/10.7554/eLife.08025
Krahe, R. and Maler, L. (2014). Neural maps in the electrosensory system of weakly electric fish. *Curr. Opin. Neurobiol.* **24**, 13-21. doi.org/10.1016/j.conb.2013.08.013
Kugino, K., Tamaru, S., Hisatomi, Y. and Sakaguchi, T. (2016). Long-duration carbon dioxide anesthesia of fish using ultra fine (nano-scale) bubbles. *PloS ONE* **11**, e0153542. doi:10.1371/journal.pone.0153542
Lettvin, J. Y., Maturana, H. R., McCulloch, W. S. and Pitts, W. H. (1959). What the Frog's Eye Tells the Frog's Brain. *Proceedings of the IRE* **47**, 1940-1951. doi:10.1109/JRPROC.1959.287207
Lissmann, H. W. (1958). On the function and evolution of electric organs in fish. *J. Exp. Biol.* **35**, 156-191.
Lissmann, H. W. and Machin, K. E. (1958). The mechanism of object location in *Gymnarchus niloticus* and similar fish. *J. Exp. Biol.* **35**, 451-486.
Madison, D. V. and Nicoll, R. A. (1984). Control of the repetitive discharge of rat CA 1 pyramidal neurones in vitro. *J. Physiol.* **354**, 319-331. doi:10.1113/jphysiol.1984.sp015378
Maler, L. (1979). The posterior lateral line lobe of certain gymnotoid fish: Quantitative light microscopy. *J. Comp. Neurol.* **183**, 323-363. doi:10.1002/cne.901830208
Maler, L. (2009a). Receptive field organization across multiple electrosensory maps.I. Columnar organization and estimation of receptive field size. *J. Comp. Neurol.* **516**, 376-393. doi:10.1002/cne.22124
Maler, L. (2009b). Receptive field organization across multiple electrosensory maps. II. Computational analysis of the effects of receptive field size on prey localization. *J. Comp. Neurol.* **516**, 394-422. doi:10.1002/cne.22120
Maler, L. and Mugnaini, E. (1994). Correlating gamma aminobutyric acidergic circuits and sensory function in the electrosensory lateral line lobe of a gymnotiform fish. *J. Comp. Neurol.* **345**, 224-252. doi:10.1002/cne.903450206
Maler, L., Sas, E. K. and Rogers, J. (1981). The cytology of the posterior lateral line lobe of high–frequency weakly electric fish (gymnotidae): Dendritic differentiation and synaptic specificity in a simple cortex. *J. Comp. Neurol.* **195**, 87-139. doi.org/10.1002/cne.901950107
Maler, L., Sas, E., Carr, C. E. and Matsubara, J. (1982). Efferent projections of the posterior lateral line lobe in gymnotiform fish. *J. Comp. Neurol.* **211**, 154-164. doi:10.1002/cne.902110205
Matsushita, A., Pyon, G. and Kawasaki, M. (2012). Time disparity sensitive behavior and its neural substrates of a pulse-type gymnotiform electric fish, Brachyhypopomus gauderio. *J. Comp. Physiol. A* **199**, 583-599. doi:10.1007/s00359-012-0784-4
Meek, J., Grant, K. and Bell, C. (1999). Structural organization of the mormyrid electrosensory lateral line lobe. *J. Exp. Biol.* **202**, 1291-1300.
Mehaffey, W. H., Fernandez, F. R., Doiron, B. and Turner, R. W. (2008a). Regulation of somatic firing dynamics by backpropagating dendritic spikes. *J. Physiol. Paris* **102**, 181-194. doi:10.1016/j.jphysparis.2008.10.011
Mehaffey, W. H., Ellis, L. D., Krahe, R., Dunn, R. J. and Chacron, M. J. (2008b). Ionic and neuromodulatory regulation of burst discharge controls frequency tuning. *J. Physiol. Paris* **102**, 195-208. doi:10.1016/j.jphysparis.2008.10.019
Mehaffey, W. H., Fernandez, F. R., Rashid, A. J., Dunn, R. J. and Turner, R. W. (2006). Distribution and function of potassium channels in the electrosensory lateral line lobe of weakly electric apteronotid fish. *J. Comp. Physiol. A* **192**, 637. doi:10.1007/s00359-006-0103-z
Migliaro, A., Caputi, A. A. and Budelli, R. (2005). Theoretical analysis of pre-receptor image conditioning in weakly electric fish. *PLoS Comput. Biol.* **1**, 0123-0131. doi:10.1371/journal.pcbi.0010016
Migliore, M. and Shepherd, G. M. (2005). An integrated approach to classifying neuronal phenotypes. *Nat. Rev. Neurosci.* **6**, 810-818. doi:10.1038/nrn1769
Mohr, C., Roberts, P. D. and Bell, C. C. (2003). The mormyromast region of the mormyrid electrosensory lobe. I. Responses to corollary discharge and electrosensory stimuli. *J. Neurophysiol.* **90**, 1193-1210. doi:10.1152/jn.00211.2003
Moller, P. (1995). *Electric Fishes: History and Behavior*. Springer.
Nelson, M. E. and MacIver, M. A. (2006). Sensory acquisition in active sensing systems. *J. Comp. Physiol. A* **192**, 573-586. doi:10.1007/s00359-006-0099-4
Nogueira Borde, J. (2011). Papel de las propiedades de una "one-spike-neuron" en la implementación de un filtro sensorial. Doctoral Thesis, Universidad de la República (Uruguay), Facultad de Ciencias. https://hdl.handle.net/20.500.12008/6460
Nogueira, J. and Caputi, Á. A. (2011). Timing actions to avoid refractoriness: A simple solution for streaming sensory signals. *PLoS ONE* **6**, e22159. doi:10.1371/journal.pone.0022159
Nogueira, J. and Caputi, A. A. (2013). From the intrinsic properties to the functional role of a neuron phenotype: An example from electric fish during signal trade-off. *J. Exp. Biol.* **216**, 2380-2392. doi:10.1242/jeb.082651
Nogueira, J. and Caputi, A. A. (2014). Pharmacological study of the one spike spherical neuron phenotype in *Gymnotus omarorum*. *Neuroscience* **258**, 347-354. doi:10.1016/j.neuroscience.2013.11.021
Nogueira, J., Castelló, M. E. and Caputi, A. A. (2006). The role of single spiking spherical neurons in a fast sensory pathway. *J. Exp. Biol.* **209**, 1122-1134. doi:10.1242/jeb.02080
Pereira, A. C. (2016). Evidencias de la naturaleza háptica del sentido eléctrico activo en peces. *PhD thesis*, PEDECIBA, Facultad de Ciencias, Universidad de la República Oriental del Uruguay. https://hdl.handle.net/20.500.12008/10228
Pereira, A. C. and Caputi, A. A. (2010). Imaging in electrosensory systems. *Interdiscip. Sci.* **2**, 291-307. doi:10.1007/s12539-010-0049-2
Pereira, A. C., Centurión, V. and Caputi, A. A. (2005). Contextual effects of small environments on the electric images of objects and their brain evoked responses in weakly electric fish. *J. Exp. Biol.* **208**, 961-972. doi:10.1242/jeb.01481
Pereira, A. C., Rodríguez-Cattáneo, A. and Caputi, A. A. (2014). The slow pathway in the electrosensory lobe of Gymnotus omarorum: Field potentials and unitary activity. *J. Physiol. Paris* **108**, 71-83. doi:10.1016/j.jphysparis.2014.07.005
Ramón y Cajal, and De Castro, (1933). *Elementos de Técnica Micrográfica del Sistema Nervioso*. Salvat editores S.A.
Rasnow, B. K. (1994). The electric field of a weakly electric fish. *PhD thesis*, California Institute of Technology, USA. https://resolver.caltech.edu/CaltechTHESIS:05162013-153557999
Ratliff, J., Marder, E. and O'Leary, T. (2018). Neural circuit robustness to acute, global physiological perturbations. *bioRxiv*. doi:10.1101/480830
Reichardt, W. and Poggio, T. (1976). Visual control of orientation behaviour in the fly Part I. A quantitative analysis. *Q. Rev. Biophys.* **9**, 311-375. doi:10.1017/S0033583500002523
Réthelyi, M. and Szabo, T. (1973). Neurohistological analysis of the lateral lobe in a weakly electric fish, *Gymnotus carapo* (Gymnotidae, Pisces). *Exp. Brain Res.* **18**, 323-339. doi:10.1007/BF00239103
Richer-de-Forges, M. M., Crampton, W. G. and Albert, J. S. (2009). A new species of Gymnotus (Gymnotiformes, Gymnotidae) from Uruguay: description of a model species in neurophysiological research. *Copeia* **2009**, 538-544.
Rodríguez-Cattaneo, A. (2017). Análisis celular y circuital de un filtro neural adaptativo de procesamiento de imágenes. PhD thesis, PEDECIBA, Facultad de Ciencias. Universidad de la República Oriental del Uruguay. https://hdl.handle.net/20.500.12008/19428.
Rodríguez-Cattáneo, A., Aguilera, P. A. and Caputi, A. A. (2017). Waveform sensitivity of electroreceptors in the pulse-type weakly electric fish *Gymnotus omarorum*. *J. Exp. Biol.* **220**, 1663-1673. doi:10.1242/jeb.153379
Rodríguez-Cattáneo, A., Pereira, A., Aguilera, P. and Caputi, Á. A. (2020). Tethered unitary recordings suggest a spike-timing electrosensory code in the electrosensory lobe of Gymnotus omarorum. *Exp. Results* **1**, E17. doi:10.1017/exp.2020.20
Saunders, J. and Bastian, J. (1984). The physiology and morphology of two types of electrosensory neurons in the weakly electric fishApteronotus leptorhynchus. *J. Comp. Physiol. A* **154**, 199-209. doi:10.1007/BF00604985
Schiller, P., Sandell, J. and Maunsell, J. (1986). Functions of the ON and OFF channels of the visual system. *Nature* **322**, 824-825. doi:10.1038/322824a0
Schlegel, P. A. (1973). Perception of objects in weakly electric fish Gymnotus carapo as studied in recordings from rhombencephalic neurons. *Exp. Brain Res.* **18**, 340-354. doi:10.1007/BF00239104
Shumway, C. A. (1989). Multiple electrosensory maps in the medulla of weakly electric gymnotiform fish. II. Anatomical differences. *J. Neurosci.* **9**, 4400-4415. doi:10.1523/jneurosci.09-12-04400.1989
Sotelo, C., Réthelyi, M. and Szabo, T. (1975). Morphological correlates of electrotonic coupling in the magnocellular mesencephalic nucleus of the weakly electric fish *Gymnotus carapo*. *J. Neurocytol.* **4**, 587-607. doi:10.1007/BF01351539
Stoddard, P. K. (1997). Detection of multiple stimulus features forces a trade-off in the pyramidal cell network of a gymnotiform electric fish's electrosensory lateral line lobe. *J. Comp. Physiol.* **182**, 103-113. doi:10.1007/s003590050162
Turner, R. W. and Maler, L. (1999). Oscillatory and burst discharge in the apteronotid electrosensory lateral line lobe. *J. Exp. Biol.* **202**, 1255-1265.
Turrigiano, G., Abbott, L. F. and Marder, E. (1994). Activity-dependent changes in the intrinsic properties of cultured neurons. *Science*, **264**, 974-977. doi:10.1126/science.8178157
von der Emde, G. and Bleckmann, H. (1992). Differential responses of two types of electroreceptive afferents to signal distortions may permit capacitance measurement in a weakly electric fish, Gnathonemus petersii. *J. Comp. Physiol. A* **171**, 683-694. doi:10.1007/BF00194116
Watson, D. and Bastian, J. (1979). Frequency response characteristics of electroreceptors in the weakly electric fish, Gymnotus carapo. *J. Comp. Physiol.* **134**, 191-202. doi:10.1007/BF00610394
Wright, P. G. (1958). An electrical receptor in fishes. *Nature* **181**, 64-65. doi:10.1038/181064a0